两个 d^{10} 金属配位聚合物的合成、结构及对2,4,6-三硝基苯酚的选择性检测

徐 涵[1] 潘兆瑞*[,2]
([1]黄山学院化学化工学院,黄山 245041)
([2]南京晓庄学院环境科学学院,南京 211171)

摘要:以4,4′-二(1-咪唑基)苯硫醚(BIDPT),4,4′-羧基二苯胺(H_2aba),5-氧乙酸间苯二酸(H_3OABDC),$Zn(NO_3)_2·6H_2O$ 和 $Cd(NO_3)_2·6H_2O$ 为原料,用溶剂热法合成了2个配位聚合物$[Zn(BIDPT)(aba)]_n$ (**1**)和$[Cd(BIDPT)(HOABDC)]_n$ (**2**)。利用X射线单晶衍射、红外、元素分析、热重分析和X射线粉末衍射对其进行了表征。单晶X射线衍射研究发现配合物**1**为具有二重穿插的三维*dia*拓扑网络结构;配合物**2**为3-连接六边形的*hcb*二维拓扑结构,再通过氢键堆积作用形成三维超分子结构。**1**和**2**具有很好的荧光性质,硝基苯化合物对配合物**1**和**2**的荧光性质有不同程度的淬灭作用。它们都对2,4,6-三硝基苯酚的检测具有很好的灵敏性。对其淬灭机理进行了深入的研究。

关键词:配位聚合物;晶体结构;荧光;硝基苯类爆炸物
中图分类号:O614.24+1;O614.24+2 **文献标识码**:A **文章编号**:1001-4861(2018)01-0055-08
DOI:10.11862/CJIC.2018.009

Syntheses, Crystal Structures and Exceptionally Selective Detection of Picric Acid of Two Luminescent d^{10} Metal-Organic Frameworks

XU Han[1] PAN Zhao-Rui*[,2]
([1]*School of Chemistry and Chemical Engineering, Huangshan University, Huangshan, Anhui* 245041, *China*)
([2]*School of Environmental Science, Nanjing Xiaozhuang University, Nanjing* 211171, *China*)

Abstract: Two coordination polymers, namely $[Zn(BIDPT)(aba)]_n$ (**1**) and $[Cd(BIDPT)(HOABDC)]_n$ (**2**) (BIDPT=4,4′-bis(imidazol-l-yl)diphenyl thioether, H_2aba=4,4′-azanediyldibenzoic acid, H_3OABDC=5-oxyacetate isophthalic acid) have been solvothermally synthesized and characterized by infrared spectroscopy, elemental analysis, and powder X-ray diffraction. In **1**, the Zn(Ⅱ) ions are linked by BIDPT and aba^{2-} ligands to give a 2-fold interpenetrating 3D frameworks with $\{6^6\}$ *dia* topology. Compound **2** can be viewed as a 3-connected *hcb* net with the point symbol of $\{6^3\}$ and extended into a three-dimensional supramolecule through hydrogen bonds. Complexes **1** and **2** show strong luminescence and their luminescence could be quenched by a series of nitroaromatic explosives. Importantly, they exhibit very highly sensitive and selective detection of picric acid compared to other nitroaromative explosives. The quenching mechanisms are also deeply studied. CCDC: 1538448, **1**; 1416600, **2**.

Keywords: coordination polymer; crystal structre; photoluminescence; nitroaromatic explosives

Rapid and selective detection of nitroaromatic explosives has immense interest because of the increasing concern about environment security. Many traditional ways have been developed to detect

收稿日期:2017-06-30。收修改稿日期:2017-09-11。
国家自然科学基金青年基金(No.21301094)和安徽高校省级自然科学研究基金(No.KJHS2017B05)资助项目
*通信联系人。E-mail:pzr_2006@163.com;会员登记号:S410800067A。

nitroaromatic explosives, such as ion mobility spectrometry, gas chromatography coupled with mass spectrometry, surface-enhanced Raman spectroscopy, X-ray imaging and other analysis methods[1-3]. These methods usually have high sensitivity and selectivity, but the defects are time-consuming, not easy to operate and high cost. Recently, significant progress has been made in the application of luminescent metal-organic frameworks (MOFs) for detection of nitroaromatic explosives due to their low cost, easy synthesis, and easy modification. For example, Zhou et al. reported a luminescent Eu(Ⅲ) MOF, which exhibited selective sensing of 2,4-dinitrotolunen (2,4-DNT) with a high K_{sv} value (1.58×10^3 L·mol^{-1})[4]. Wang et al. reported a Cd MOF for the detection of 4-nitrophenol (4-NP) with the high K_{sv} value (6.74×10^4 L·mol^{-1}) and low detection limit (34.48 μg·L^{-1})[5]. Shi et al. reported two stable Zn MOFs for the detection of picric acid (PA) with K_{sv} values of 2.40×10^4 L·mol^{-1} and 2.46×10^4 L·mol^{-1}, respectively[6].

Herein, two luminescent compounds [Zn(BIDPT)(aba)]$_n$ (**1**) and [Cd(BIDPT)(HOABDC)]$_n$ (**2**), have been successfully synthesized for sensitive detection of nitroaomative explosives through photoluminescence quenching. Notably, **1** and **2** exhibit highly selective detection of PA. Quenching mechanism also has been studied deeply herein.

1 Experimental

1.1 Materials and measurement

All starting materials and solvents used during the experiments were purchased commercially without further purification. Ligand BIDPT was synthesized as reported in the literature[7]. Elemental analyses (C, H and N) were carried out on a Perkin-Elmer model 240C elemental analyzer. The FT-IR spectra were obtained on a Bruker Vector 22 FTIR spectrophotometer by using KBr pellets in the range of 400~4 000 cm^{-1}. Thermogravimetric analysis (TGA) was conducted on a NETZSCH STA 449C analyzer. Powder X-ray diffraction (PXRD) measurements were performed on a Bruker D8 Advance X-ray diffraction using Cu $K\alpha$ radiation (λ=0.154 18 nm, 2θ=5°~50°) in which the X-ray tube was operated at 40 kV and 40 mA. Solid-state luminescent spectra were recorded with a SHIMADZU VF-320 X-ray fluorescence spectrophotometer at room temperature.

1.2 Syntheses of compounds

[Zn(BIDPT)(aba)]$_n$ (**1**). A mixture of $Zn(NO_3)_2\cdot6H_2O$ (29.5 mg, 0.1 mmol), BIDPT (34.0 mg, 0.1 mmol) and H_2aba (25.6 mg, 0.1 mmol) was dissolved in 9 mL H_2O/CH_3OH (1:2, *V*/*V*). The final mixture was placed in a Parr Teflon-lined stainless steel vessel (15 mL) under autogenous pressure and heated at 120 ℃ for three days. Light brown prism crystals were obtained. The yield of the reaction was *ca.* 41% based on BIDPT ligand. Anal. Calcd. for $C_{32}H_{22}ZnN_5O_4S$(%): C, 60.19; H, 3.45; N, 10.97. Found (%): C, 60.32; H, 3.32; N, 10.81. IR (KBr, cm^{-1}): 3 403 (m), 3 131(s), 1 687 (s), 1 596 (s), 1 518 (m), 1 400 (s), 1 304(m), 1 173(m), 1 127(w), 1 063(m), 964(m), 879(m), 827 (m), 780(s), 655 (w), 551(w).

[Cd(BIDPT)(HOABDC)]$_n$ (**2**). A mixture of $Cd(NO_3)_2\cdot6H_2O$ (30.8 mg, 0.1 mmol), BIDPT (34.0 mg, 0.1 mmol) and H_3OABDC (24.0 mg, 0.1 mmol) was dissolved in 5 mL of DMF/CH_3CN/H_2O (V_{DMF}:V_{CH_3CN}:V_{H_2O}=1:2:2). The final mixture was placed in a Parr Teflon-lined stainless steel vessel (15 mL) under autogenous pressure and heated at 95 ℃ for three days. Colorless block crystals were obtained. The yield of the reaction was ca. 46% based on BIDPT ligand. Anal. Calcd. for $C_{28}H_{20}CdN_4O_7S$(%): C, 50.23; H, 2.99; N, 8.37. Found (%): C, 50.20; H, 3.04; N, 8.32. IR (KBr, cm^{-1}): 3 405(m), 3 130(s), 1 715(m), 1 662(m), 1 587(m), 1 513(s), 1 401(s), 1 386(s), 1 307(m), 1 277 (m), 1 127(m), 1 063(w), 962(w), 936(w), 827(m), 779 (w), 766(w), 649(w), 551(w).

1.3 Single crystal X-ray crystallography

Intensity data were collected with a Bruker SMART CCD diffractometer using graphite-monochromated Mo $K\alpha$ radiation (λ=0.071 073 nm) for **1** and **2**. All absorption corrections were performed using the SADABS program[8]. The structures were solved by direct methods and all non-hydrogen atoms were refined anisotropically on F^2 by the full-matrix least-squares technique using the SHELXL-97 crystallog-

raphic software package[9]. All the hydrogen atoms were generated geometrically and refined isotropically using a riding model. The details of the crystal parameters, data collection and refinements for **1** and **2** are listed in Table 1, selected bond lengths and angles are summarized in Table 2.

CCDC: 1538448, **1**; 1416600, **2**.

Table 1　Crystallographic data for 1 and 2

Compound	**1**	**2**
Empirical formula	$C_{32}H_{22}ZnN_5O_4S$	$C_{28}H_{20}CdN_4O_7S$
Formula weight	637.98	668.94
a / nm	1.819 8(4)	0.835 7(5)
b / nm	1.376 4(3)	2.483 1(1)
c / nm	2.340 3(5)	1.329 5(7)
β / (°)		107.473(1)
Crystal system	Orthorhombic	Monoclinic
Space group	*Pbca*	$P2_1/c$
V / nm^3	5.862 0(2)	2.631 6(3)
Z	8	4
D_c / (g·cm^{-3})	1.446	1.688
Size / mm	0.30×0.24×0.22	0.28×0.24×0.20
μ / mm^{-1}	0.956	0.966
F(000)	2 616	1 344
θ_{min}, θ_{max} / (°)	1.74, 27.52	1.64, 27.49
Goodness of fit on F^2	1.088	1.018
Reflection collected	37 017	17 599
Independent reflection (R_{int})	6 714 (0.133 3)	6 027 (0.031 8)
R_1, wR_2 [$I>2\sigma(I)$]	0.058 7, 0.126 6	0.032 5, 0.069 7
R_1, wR_2 (all data)	0.164 1, 0.157 8	0.047 2, 0.075 8
$(\Delta\rho)_{max}$, $(\Delta\rho)_{min}$ / (e·nm^{-3})	849, −339	466, −447

Table 2　Selected bond distances (nm) and bond angles (°) of 1 and 2

			1		
Zn(1)-N(1)	0.203 3(4)	Zn(1)-O(2)#1	0.193 2(4)	Zn(1)-N(4)#2	0.202 8(4)
Zn(1)-O(4)	0.212 7(4)	Zn(1)-O(3)	0.238 2(4)		
O(2)#1-Zn(1)-N(1)	118.37(19)	O(2)#1-Zn(1)-N(4)#2	108.35(16)	N(1)-Zn(1)-N(4)#2	102.13(15)
O(2)#1-Zn(1)-O(4)	93.61(16)	N(1)-Zn(1)-O(4)	91.70(16)	N(4)#2-Zn(1)-O(4)	143.64(15)
O(2)#1-Zn(1)-O(3)	116.9(2)	N(1)-Zn(1)-O(3)	116.15(16)	N(4)#2-Zn(1)-O(3)	88.34(15)
O(4)-Zn(1)-O(3)	55.55(14)				
			2		
Cd(1)-N(1)#1	0.222 6(2)	Cd(1)-O(2)#2	0.220 4(2)	Cd(1)-N(4)	0.223 9(2)
Cd(1)-O(4)	0.228 9(2)	Cd(1)-O(5)	0.245 6(2)		
O(2)#2-Cd(1)-N(1)#1	117.66(8)	O(2)#2-Cd(1)-N(4)	110.16(8)	N(1)#1-Cd(1)-N(4)	100.05(8)
O(2)#2-Cd(1)-O(4)	97.77(7)	N(1)#1-Cd(1)-O(4)	93.96(8)	N(4)-Cd(1)-O(4)	137.64(7)
O(2)#1-Cd(1)-O(5)	115.06(8)	N(1)#1-Cd(1)-O(5)	121.32(8)	N(4)-Cd(1)-O(5)	84.18(7)
O(4)-Cd(1)-O(5)	54.76(6)				

Symmetry codes: #1: $-x-1/2, -y+2, z+1/2$; #2: $x-1/2, -y+5/2, -z+1$ for **1**; #1: $-x, 1-y, 1-z$; #2: $x, 3/2-y, -1/2+z$ for **2**.

2 Results and discussion

2.1 Structures description

2.1.1 Crystal structure analysis of $[Zn(BIDPT)(aba)]_n$ (**1**)

The X-ray crystallographic analysis shows that compound **1** crystallizes in the orthorhombic crystal system with the *Pbca* space group. The asymmetric unit contains one Zn(Ⅱ) cation, one BIDPT ligand and one aba^{2-} ligand. As shown in Fig.1, the Zn(Ⅱ) cation locates in a $\{ZnN_2O_3\}$ distorted square-pyramidal geometry made up of two nitrogen atoms and three carboxylate oxygen atoms from two aba^{2-} ligands. The Zn-O lengths are in the range of 0.193 2 (4)~0.238 2(4) nm, while the Zn-N bond lengths are in the range of 0.202 8(4)~0.203 3(4) nm, which are in the normal range[10-11]. The aba^{2-} anions join neighboring Zn(Ⅱ) cations center to generate a 1D right-handed helical chain structure. The BIDPT ligands link the Zn(Ⅱ) cations to form another 1D right-handed helical chain structure (Fig.2). Both of the adjacent right-handed helical chains are arranged like a cross shape, leading to the formation of a 3D framework (Fig.3a). The 3D structure can be clarified as a 4-connected diamond (*dia*) lattice by considering Zn(Ⅱ) cations as the connected nodes and all ligands as the 2-connected spacers (Fig.3b). Therefore, the whole structure can thus be represented as a *dia* topology with a point symbol of $\{6^6\}$.

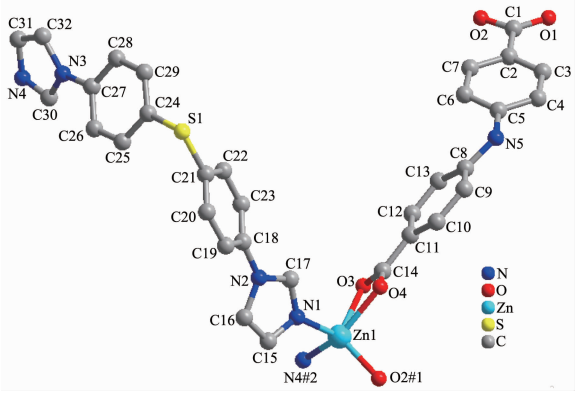

All hydrogen atoms were omitted for clarity; Symmetry codes: #1: $-x-1/2, -y+2, z+1/2$; #2: $x-1/2, -y+5/2, -z+1$

Fig.1 Coordination environment of the Zn(Ⅱ) cation in **1**

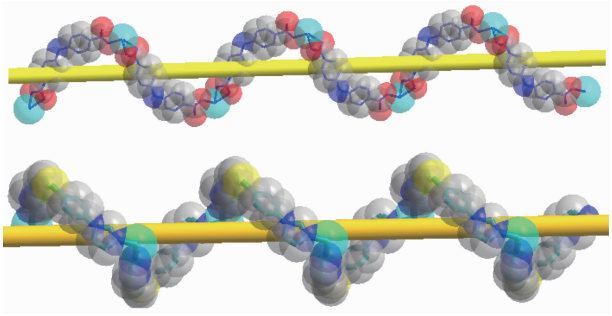

Fig.2 View of two types of right-handed helical chains constructed by aba^{2-} and Zn(Ⅱ), BIDPT and Zn(Ⅱ)

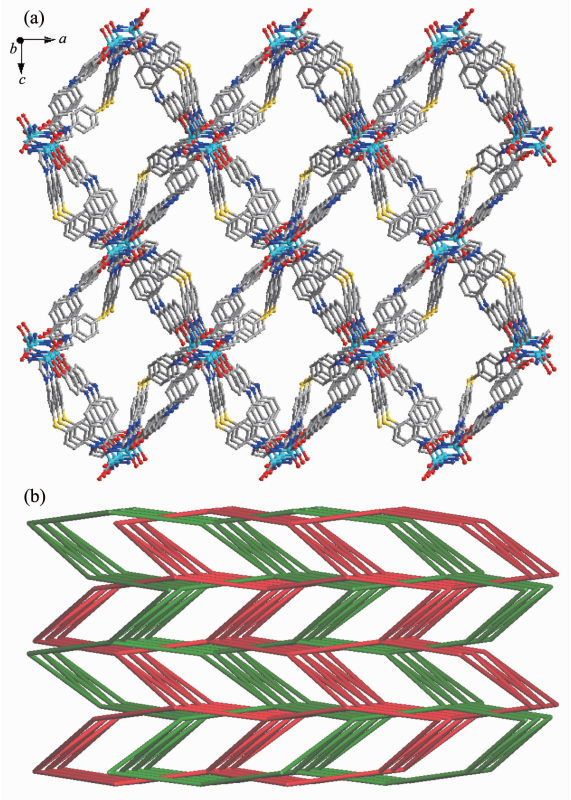

Fig.3 (a) View of the 3D framework of **1** along the *b* axis; (b) Two-fold interpenetrating 3D *dia*-type topology of **1**

2.1.2 Crystal structure analysis of $[Cd(BIDPT)(HOABDC)]_n$ (**2**)

Single-crystal X-ray structural analysis reveals that compound **2** crystallizes in the monoclinic crystal system with the $P2_1/c$ space group and features a 2D undulated layered structure. The asymmetric unit of **2** is composed of one crystallographically independent Cd(Ⅱ) cation, one BIDPT ligand and one partially deprotonated $HOABDC^{2-}$ ligand (Fig.4). Cd(Ⅱ) is coordinated by two nitrogen atoms from two BIDPT ligands (Cd-N 0.222 6(2)~0.223 9(2) nm), two oxygen atoms from one rigid carboxyl group and one oxygen atom

from one flexible carboxyl group of two individual $HOABDC^{2-}$ ligands (Cd-O 0.220 4(2)~0.245 6(2) nm). The Cd-O/N bong lengths are all normal and comparable to other Cd(Ⅱ) compounds[12-13]. The rigid and flexible carboxylate groups of $HOABDC^{2-}$ ligand link the Cd(Ⅱ) cations to form one infinite 1D zigzag chain with the Cd…Cd distance of 0.686 2(4) nm and Cd…Cd…Cd angle of 151.256(4)° (Fig.5a). Two BIDPT ligands link two Cd(Ⅱ) cations to form an approximately rhombus $[Cd_2(BIDPT)_2]$ 32-membered metallamacrocycle (Fig.5b). The supplementary interior angles are 80.966° and 99.034°, respectively. In the metallamacrocycle, the N…Cd…N angle is 100.1°. Furthermore, a 2D undulated network is formed by the cross-link between the metallamacrocycles and the 1D zigzag chains (Fig.6a). By taking Cd(Ⅱ) ions as 3-connected nodes, and organic ligands as linkers, this 2D sheet can be viewed as a 3-connected *hcb* net with the point symbol of $\{6^3\}$ (Fig.6b). Further, these layers stack in an AAA model to construct a 3D supramolecular framework by intermolecular hydrogen bond (O6-H6A…O1#1) formed in the adjacent layers (Fig.7).

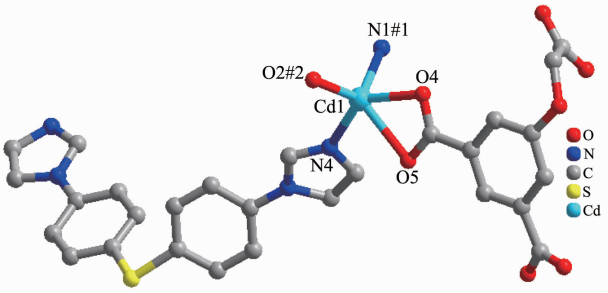

All hydrogen atoms were omitted for clarity; Symmetry codes: #1: $-x$, $1-y$, $1-z$; #2: x, $3/2-y$, $-1/2+z$

Fig.4　Coordination environment of the Cd(Ⅱ) cation in **2**

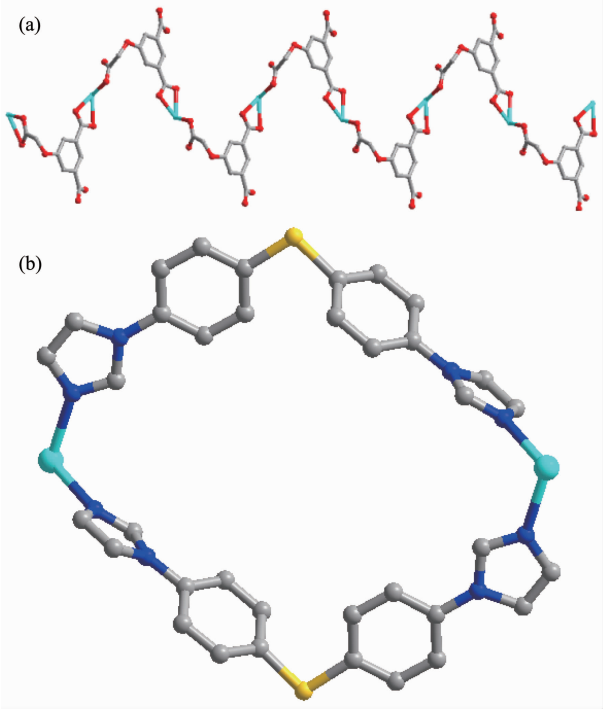

Fig.5　(a) Infinite 1D linear chain formed by Cd(Ⅱ) cations and $HOABDC^{2-}$ ligands; (b) Rhombus $[Cd_2(BIDPT)_2]$ metallamacrocycle

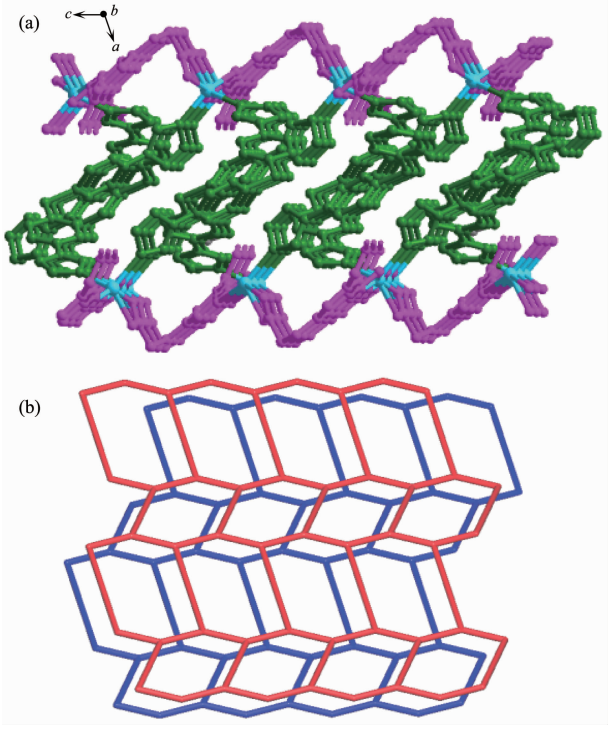

Fig.6　(a) 2D network of 2 viewed from the b axis direction (b) Schematic representation of 3-connected *hcb* net

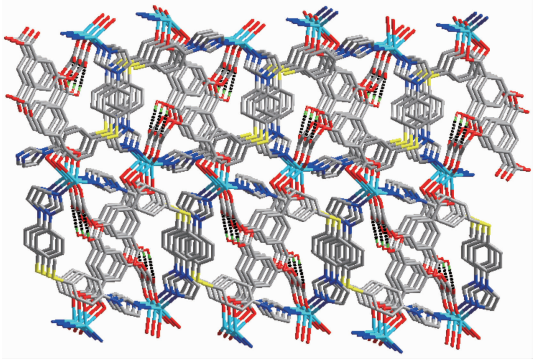

Hydrogen bond: black dashed line

Fig.7　View of the 3D supramolecular framework incorporating hydrogen bonds of **2**

2.2 Thermal stability and powder X-ray diffraction (PXRD)

To examine the thermal stabilities of these two compounds, TGA were carried out. As shown in Fig.8, the TGA study of compound **1** indicates no obvious weight loss from 25 to 250 ℃, suggesting that the frameworks are thermally stable. For **2**, no obvious weight loss is observed from 25 to 330 ℃, after that the decomposition of **2** starts. This phenomenon may be attributed to the coexistence of strong hydrogen bonding interaction and coordination interaction[14].

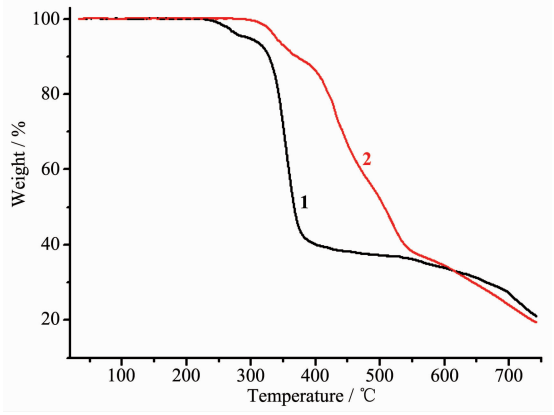

Fig.8 TG curves of compounds **1** and **2**

To confirm the purity of **1** and **2**, powder X-ray diffraction analysis (PXRD) were carried out. The experimental spectra of them are nearly consistent with their simulated spectra (Fig.9), which indicates that **1** and **2** have been successfully obtained as pure crystalline.

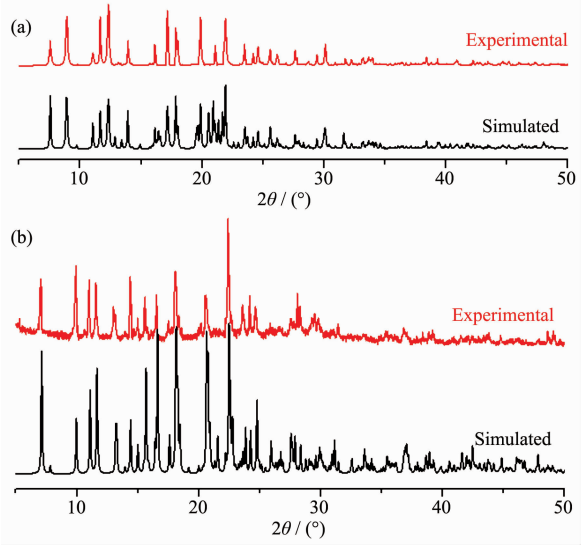

Fig.9 PXRD curves of compounds **1** (a) and **2** (b)

2.3 Luminescent property and determination of nitroaromatic compounds

To examine their luminescence properties, the solid-state luminescence of **1** and **2** are investigated at room temperature. The emission peaks of **1** and **2** appear at 510 and 525 nm, respectively, which may be attributed to the ligation of the ligand to the metal center in d^{10} compounds[15] (Fig.10). The luminescence of **1** and **2** motivated us to investigate its potential application in the detection of sensing small molecules. Considering environmental security and the strong emission of **1** and **2**, we investigate their possibility of sensing nitroaromatic explosives, including 2,4-DNT, PA, 4-NP, 2,4-dinitrophenol (2,4-DNP), nitrobenzene (NB), 3-nitrophenol (3-NP), 1,3-dintrobenzene (1,3-DNB), 4-nitrotoluene (NT), 1,4-dintrobenzene (1,4-DNB); in detail, a series of suspensions of **1** and **2** in dimethylformamide (DMF) with gradually increasing concentrations of nitroaromatic explosives in DMF solution (5 mmol·L^{-1}) were prepared to monitor the photolumonescence response. As shown in Fig.11, the order of quenching efficiency for **1** is PA > 3-NP > 1,4-DNB > NT > 2,4-DNP > 2,4-DNT > 1,3-DNB > 4-NP > NB, and the quenching efficiency for **2** is PA > 1,4-DNB > NT > 2,4-DNP > 4-NP > 1,3-DNB > 2,4-DNT > NB > 3-NP. To our excitement, there were significant luminescence attenuation with quenching rate of 64.3% for **1** and 61.0% for **2** in the presence of PA with the concentration of 50 μmol ·L^{-1}.

The titration curves showed that emission intensity of **1** and **2** both decreased with increasing concentration of PA from 2.5 to 150.0 μmol·L^{-1} (Fig.

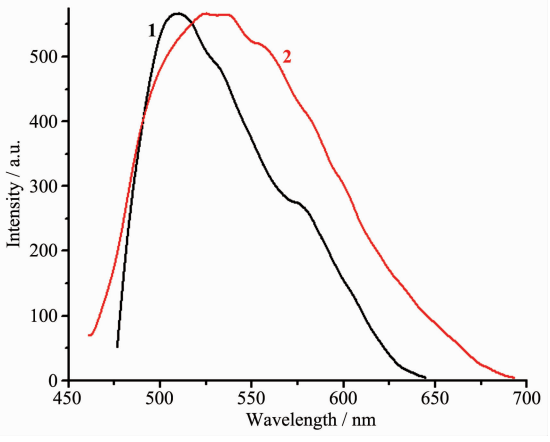

Fig.10 Solid-state photoluminescent spectra for **1** and **2**

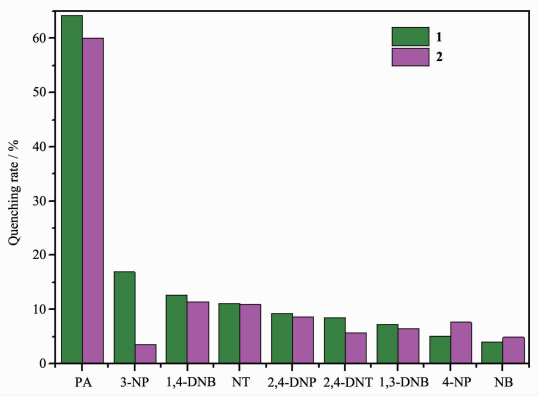

Fig.11　Quenching rates of photoluminescence for **1** and **2** upon addition of different explosive analytes with a concentration of 50 μmol·L^{-1}

12a,c). The photoluminescence quenching efficiency can be quantitatively explained by the Stern-Volmer (SV) equation: $I_0/I=1+K_{sv}c_{PA}$, where I_0 and I are the luminescence intensities of **1** and **2** DMF suspens-ions before and after the addition of PA, respectively; K_{sv} is the quenching constant (L·mol^{-1}), and c_{PA} is the concentration of PA. As shown in Fig.12b,d, at low concentrations, the SV plots of PA display nearly linear (R^2=0.992 for **1** and R^2=0.994 for **2**), the K_{sv} values were calculated to be 3.46×10^4 L·mol^{-1} for **1** and 2.28×10^4 L·mol^{-1} for **2**, which is comparable to those in well-designed solution base organic compounds for sensing of PA[16-19]. However, at higher concentration, the SV lots subsequently deviate from linearity and bend upward, which may be due to the self-absorption[20]. Low detection concentration and high quenching constant of PA show **1** and **2** can easily detect a trace quantity of PA. The mechanism of selective sensing of explosives based on coordination polymers (CPs) is not very clear, maybe the resonance energy transfer makes PA exhibit high photoluminescence quenching compared to others.

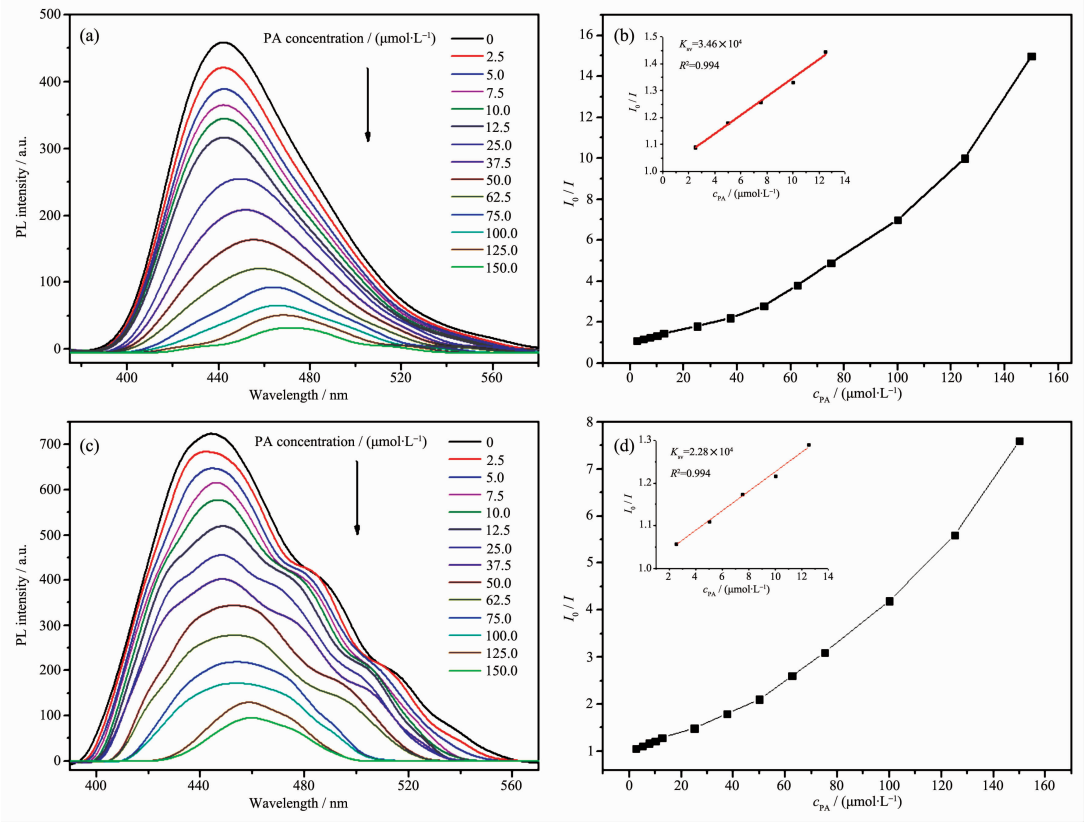

Inset: enlarged view of a selected area in (b) and (d)

Fig.12　(a) Concentration-dependent luminescence quenching of **1** after adding different concentrations of PA; (b) Stern-Volmer plot of I_0/I versus PA concentration in the **1** aqueous suspension; (c) Concentration-dependent luminescence quenching of **2** after adding different concentrations of PA; (d) Stern-Volmer plot of I_0/I versus PA concentration in the **2** aqueous suspension

2.4 Mechanism of sensing nitroaromatic explosives for 1 and 2

The possible reason for the quenching may be the resonance energy transfer mechanism[21]. The non-linearity of the SV plot for PA suggests that such an energy transfer mechanism exists in the photoluminescence quenching process. The spectral overlap between the UV-Vis absorption spectra of nitroaromatic analytes and the emission spectra of **1** and **2** were also checked. As shown in Fig.13, the absorption spectrum of PA has an effective overlap with the emission spectra of **1** and **2**, so the resonance energy transferred between CPs and PA can be proved[22]. As a result, resonance energy transfer makes PA exhibits high level of photoluminescence quenching compared to other nitroaromatic analytes.

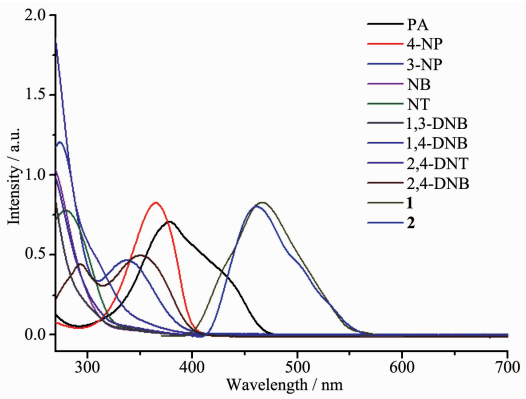

Fig.13 Spectral overlap between UV-Vis spectra of explosive analytes and the emission spectra of **1** and **2** in DMF

3 Conclusions

In summary, two new CPs with different framework structures have been successfully constructed under hydrothermal conditions. Moreover, **1** and **2** show strong luminescence and their luminescence could be quenched by a series of nitroaromatic explosives. Importantly, they exhibits very highly sensitive and selective detection of picric acid compared to other nitroaromative explosives due to the resonance transfer. Our work provides a rational strategy for design and synthesis of MOF-based sensors for selective and sensitive detection of one nitroaromatic explosive from other nitroaromatic explosives.

References:

[1] Anferov V P, Moajoukhine G V, Fisher R. *Rev. Sci. Instrum.*, **2000**,**71**:1656-1659

[2] Ye J, Zhao L, Bogale R G, et al. *Chem. Eur. J.*, **2015**,**21**: 2029-2037

[3] Moore D S. *Rev. Sci. Instrum.*, **2004**,**75**:2499-2512

[4] Zhou X H, Li L, Li H H, et al. *Dalton Trans.*, **2013**,**42**:12403-12409

[5] Wang Z J, Qin L, Chen J X, et al. *Inorg. Chem.*, **2016**,**55**: 10999-11005

[6] Shi Z Q, Guo Z J, Zheng H G. *Chem. Commun.*, **2015**,**51**: 8300-8303

[7] Hu J S, Shang Y J, Yao X Q, et al. *Cryst. Growth Des.*, **2010**, **10**:4135-4142

[8] Sheldrick G M. *SADABS, Program for Empirical Absorption Correction of Area Detector Data*, University of Göttingen, Germany, **1996**.

[9] Sheldrick G M. *SHELXL*-97, *Program for X-ray Crystal Structure Refinement*, University of Göttingen, Germany, **1997**.

[10]MA De-Yun(马德运), LI Xiang(李湘), GUO Hai-Fu(郭海福), et al. *Chinese J. Inorg. Chem.*(无机化学学报), **2017**,**33** (7):1266-1272

[11]Han L J, Yan W, Chen S G, et al. *Inorg. Chem.*, **2017**,**56**: 2936-2940

[12]XU Han(徐涵), ZHENG He-Gen(郑和根). *Chinese J. Inorg. Chem.*(无机化学学报), **2015**,**31**(11):2272-2278

[13]Huang Y Q, Wang Y H, Zhao Y, et al. *Inorgan. Chim. Acta*, **2013**,**394**:164-170

[14]Huang Y Q, Cheng H D, Chen H Y, et al. *CrystEngComm*, **2015**,**17**:5690-5701

[15]Deng J H, Zhong D C, Luo X Z, et al. *Cryst. Growth Des.*, **2012**,**12**:4861-4869

[16]Chopra R, Bhalla V, Kumar M, et al. *RSC Adv.*, **2015**,**5**: 24336-24341

[17]Nagarajan V, Bag B. *Org. Biomol. Chem.*, **2014**,**12**:9510-9513

[18]Chowdhury A, Mukherjee P S. *J. Org. Chem.*, **2015**,**80**:4064-4075

[19]Wang G Y, Yang L L, Li Y, et al. *Dalton Trans.*, **2013**,**42**: 12865-12868

[20]Lan A, Li K, Wu H, et al. *Angew. Chem. Int. Ed.*, **2009**,**48**: 2334-2338

[21]Zhang C Q, Sun L B, Yan Y, et al. *Dalton Trans.*, **2015**,**44**: 230-236

[22]Xu H, Zheng H G. *Inorg. Chem. Commun.*, **2016**,**66**:51-54